THE JOURNAL OF Ammonia Energy

Available online at

jae.cardiffuniversitypress.org

ISSN **2752-7735**
The Journal of Ammonia Energy 01 (2023) 033–045

Cardiff University Press | Gwasg Prifysgol Caerdydd

The Acoustic Response of Hydrogen/Ammonia Flames

Duarte Nunes C*, Morgans AS

Department of Mechanical Engineering, Imperial College London, United Kingdom

Abstract

Ammonia is a carbon-free fuel which could be used in gas turbines. Ammonia's potential as a fuel can be improved when mixed with hydrogen. However, this could cause an increased propensity to thermoacoustic oscillations in the combustor. The acoustic response of hydrogen/ammonia flames was evaluated by calculating the flame transfer functions (FTFs). A local level set approach, combined with an incompressible velocity perturbation model, was used to calculate the flame front response to different frequencies of acoustic oscillations. The unsteady heat release rate was calculated from the flame front surface area, obtained by solving the G-equation, thereby calculating the gain and phase of the FTF. The unstretched flame speed, was obtained from experimental values and two chemical kinetic models: CRECK-NH3 and GRI-Mech3.0. The models' accuracy was assessed by comparing the modelled to experimental values from literature. CRECK-NH3 was fitter for ammonia/hydrogen modelling, as it was always within 12% of experimental values, compared to GRI-Mech3.0 which always differed by over 35%. The FTFs suggested an increase in hydrogen enrichment led to an increase in the flame acoustic response, as the gain drop off occurred at a higher frequency with higher hydrogen content. The flame acts as a low-pass filter to acoustic waves and the bandwidth of this filter (the frequency at which the gain drops off) increases with hydrogen content. This was due to higher flame speeds with higher hydrogen content. These FTFs were also compared to those of hydrogen/methane flames and the non-linear response was briefly analysed.

Received: 01st Feb 23; Accepted: 10th May 23; Published: 4th July 23

Keywords: Ammonia, Hydrogen, Thermoacoustic, Flame transfer function.

Introduction

Ammonia is a carbon-free fuel which could be used in gas turbines for a more environmentally friendly energy production. Its potential as fuel can be improved through the addition of hydrogen, as the latter has a much higher lower heating value and flame speed. Hydrogen addition, however, often leads to an increased propensity to thermoacoustic instability and oscillations [1].

Thermoacoustic instability is caused by the coupling between the unsteady heat release of the flame and the consequent acoustic oscillations. A minor disturbance to the flame will create unsteady heat release, which creates acoustic oscillations. These are reflected back from the combustor boundaries and further excite the flame, causing more unsteady heat release, and the cycle repeats itself. These instabilities lead to an initial exponential increase in oscillations until non-linear effects cause them to saturate, most likely to limit cycle oscillations. These instabilities will always lead to adverse effects [2], ranging from lower combustion efficiency to catastrophic material failure, and are therefore of major importance for gas turbine design and development.

Thermoacoustic stability can be predicted if two things are known: the behaviour of acoustic waves within the combustor as well as the response of the flame to acoustic waves. The latter can be represented through what is known as the flame transfer function (FTF). Using an FTF assumes the dominant frequency of the unsteady heat release rate response is equal to the forcing frequency [3]. The FTF is typically complex valued and contains the gain and phase shift information of the normalised unsteady heat release rate of the flame in relation to the normalised acoustic perturbations present in the flow. This linear response depends only on the frequency of the input acoustic oscillations [4].

As efforts in the decarbonisation of energy production increase, it has become more important to understand the effects of hydrogen enrichment on the performance of gas turbines [5]. Future gas turbines could also be fuelled by totally carbon-free fuels, such as ammonia and hydrogen [6], and it is therefore important to understand the thermoacoustic behaviour of these flames. To the best of the authors' knowledge, not much research has yet been conducted on the acoustic response of ammonia-fuelled flames. This was also noted by Katoch et al. [7], who conducted an experimental study on thermoacoustic instability within a specific

* Corresponding author. Tel.: +44-7767-056835. E-mail address: catarina.duarte-nunes18@imperial.ac.uk
https://doi.org/10.18573/jae.15

ammonia-hydrogen dual-fuel burner. None have yet attempted to obtain either the FTF or the flame describing function (FDF) of pure ammonia or ammonia-hydrogen flames either numerically or experimentally.

The present work evaluates the acoustic response of rich ammonia hydrogen premixed flames through numerical simulation of the flame front using a local level set approach and an incompressible flow field model [8,9]. The unstretched laminar flame speed, required for this approach, was either obtained from the literature or calculated using chemical kinetic models. The effect of several variables, such as Markstein length and flame speed, on the flame response was also assessed using the FTFs.

Background Theory

The flame transfer function (FTF) depends only on the flow perturbation frequency, ω, and is shown in equation (1). The normalised flow velocity perturbation amplitude, β, which is the flow velocity perturbation, u' normalised by the mean flow velocity, $\bar{u}$, as shown in equation (2), was kept constant for all simulations with $\beta = 0.036$. Non-linear effects are disregarded when calculating the FTFs. The FTF represents the gain and phase shift of the flame with respect to the acoustic perturbations present in the flow.

$$\mathcal{F}(\omega) = \frac{\frac{\dot{Q}'}{\bar{\dot{Q}}}}{\beta} \quad (1)$$

$$\beta = \frac{u_1'}{\overline{u_1}} \quad (2)$$

The FTF gain can be calculated by measuring the amplitude of the normalised heat release rate once it has saturated and reached the limit cycle. The FTF phase shift can be calculated through cross-correlation of the normalised heat release rate limit cycle oscillations, and the flow perturbation function (these are both periodic functions). An example of the normalised heat release rate progression in time is shown in Fig. 1 for illustrative purposes, where QRatio refers to the normalised heat release rate.

The unsteady heat release rate of the flame, $\dot{Q}'$, required to calculate the FTF, is proportional to the ratio of the perturbed flame surface area, A'_f, to the mean flame surface area, $\overline{A_f}$, as shown in equation (3) where $\bar{\dot{Q}}$ is the mean heat release rate [10].

$$\frac{\dot{Q}'}{\bar{\dot{Q}}} = \frac{A'_f}{\overline{A_f}} \quad (3)$$

The G-equation, also known as the level set approach, is one of the most popular approaches to modelling the flame front response to perturbations [4, 11-13]. G=0 is taken to represent the flame front separating the unburned gases (G<0) from the burned gases (G>0). Kinematic modelling of the flame-front in this way relies on three major assumptions [8, 11]: the flame is an infinitely thin interface, the flame is axisymmetric, and the reaction chemistry is infinitely fast. The G-equation is shown in equation (4), where $\vec{u}$ is the flow velocity vector, t is time and s_L is the stretched laminar flame speed. This method has previously been used to model acoustically perturbed methane air flames and was successfully validated with Schlieren imaging [14].

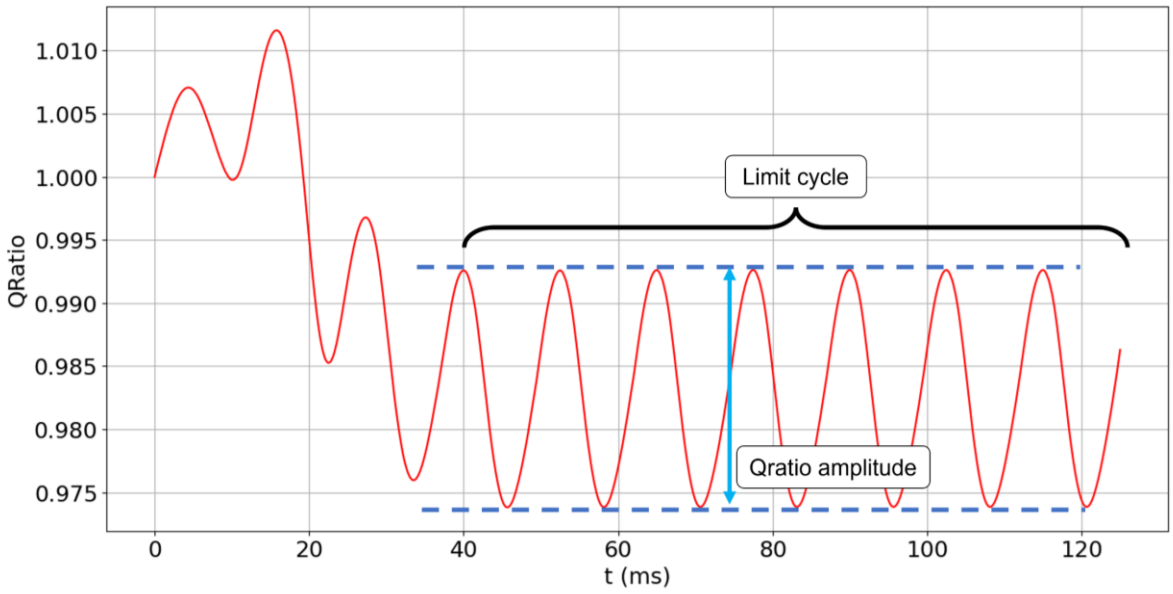

Fig. 1. Illustrative example of the progression of the normalised heat release rate of a perturbed ammonia-hydrogen fuelled flame.

$$\frac{\partial G}{\partial t} + \vec{u} \cdot \nabla G = s_L |\nabla G| \quad (4)$$

Materials and Methods

The numerical simulation relates to an axisymmetric conical premixed laminar flame, with a base diameter of D = 22 mm (burner diameter). An illustration of the simulated flame is shown in Fig. 2.

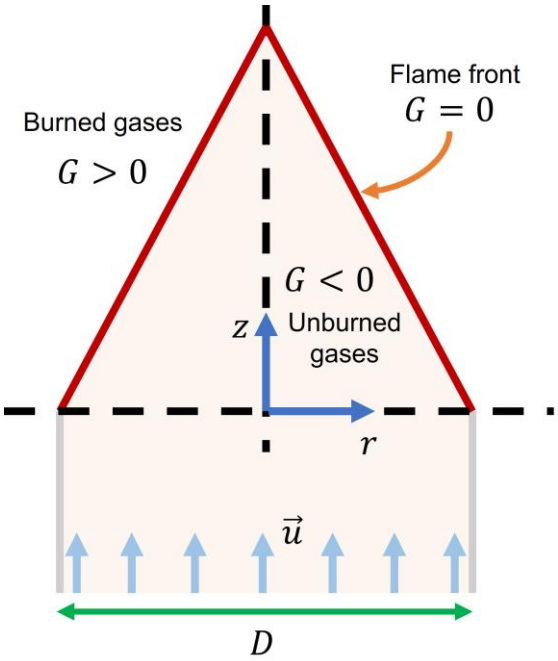

Fig. 2. Schematic of conical flame with G = 0 representing the flame front, G < 0 the unburned gases and G > 0 representing the burned gases

Each flame was defined by its hydrogen enrichment level, η, which corresponds to the amount of hydrogen present within the fuel, and its equivalence ratio, ϕ, as shown in equations (5) and (6), where X represents the relevant mole fraction and FAR the fuel to air ratio. The unburned gas temperature, T_u, was set as 293 K and the unburned gas pressure, P_u, was set as 1 atm for all simulated flames.

$$\eta = \frac{X_{H_2}}{X_{NH_3} + X_{H_2}} \quad (5)$$

$$\phi = \frac{FAR}{FAR_{stoichiometric}} \quad (6)$$

The stretched laminar flame speed, s_L, is dependent on the unstretched laminar flame speed, s_{L0}, the Markstein length, $\mathcal{L}$, and the flame stretch rate, α [9]. In this work, flame strain effects were disregarded and α was therefore only dependent on s_{L0} and local flame curvature, κ:

$$s_L = s_{L0}(1 - \mathcal{L}\kappa) \quad (7)$$

The Markstein length, $\mathcal{L}$, is a characteristic length of the same order of magnitude as the flame thickness, δ_f, and measures the effect of flame curvature on flame speed. The ratio $\mathcal{L}/\delta_f$ is called the Markstein number, $\mathcal{M}$ [15].

Once the flame was defined, its unstretched laminar flame speed, s_{L0}, was calculated from either experimental values available in the literature or through chemical kinetic models using the Python library CANTERA [16]. The local flame curvature can be calculated from the flame front shape while dummy values of $\mathcal{M}$ were used throughout this work as a previous similar study for methane-hydrogen flames suggested it had little effect on the flame response [17].

A MATLAB based script was adapted which had been previously developed by [14] for simulating acoustically perturbed methane flames by solving the G-equation using a 5th order WENO (weighted essentially non-oscillatory) scheme for spatial discretisation and a 3rd order TVD (total variation diminishing) Runge-Kutta scheme for temporal integration. The spatial and temporal grid spacing were altered for every simulation to ensure stability. An altered version of this script was previously used to simulate acoustically perturbed hydrogen-enriched methane flames [17]. This script was altered for ammonia-hydrogen flame simulations.

An incompressible flow velocity perturbation model (equations (8) and (9)) was used with the G-equation, as it has been previously shown to better capture complex flame front evolution phenomena such as flame pinch-offs [18]. In these equations, u_z is the instantaneous axial velocity, u_r the instantaneous radial velocity, k is the wave number and ω is the forcing frequency in radians. Forcing frequencies between 10 Hz and 160 Hz, in increments of 10 Hz, were used in the simulations. The mean flow velocity, $\bar{u}$, was calculated for each different fuel composition so as to maintain the constant mean heat release rate used for all simulations, $\bar{\dot{Q}} = 2.69$ kW. This value of $\bar{\dot{Q}}$ was chosen to match the one used by [17] for methane-hydrogen fuelled flames to ease comparison between the acoustic response of the ammonia and the methane flames.

$$u_z(z,t) = \bar{u} + \hat{u'}\cos(kz - \omega t) \quad (8)$$

$$u_r(r,z,t) = k\frac{r}{2}\hat{u'}\sin(kz - \omega t) \quad (9)$$

Flame speed calculation

The unstretched laminar flame speeds of the different fuel blends were obtained in two ways: through experimental values available in the

literature and through the use of two chemical kinetic mechanisms.

Very limited experimental data was available from the literature for s_{L0} of different blends of ammonia hydrogen [19-21]. Li et al. [19] utilised the Bunsen burner method to measure the flame speed of ammonia and hydrogen flames for $\eta = \{0.333, 0.385, 0.455, 0.5, 0.545, 0.6\}$ and ϕ ranging from 0.6 to 1.375, at NTP (normal temperature and pressure). Ichikawa et al. [20] measured the flame speed of spherically propagating flames using Schlieren imaging, for stoichiometric flames with η ranging from 0 to 1 and a temperature of 298 K and a pressure of 1 bar. Lee et al. [21] utilised this same method, but with $\phi = \{0.6, 0.8, 1, 1.25, 1.67\}$ and η of either 0.1, 0.3 or 0.5. The differences in temperature and pressure between [19], [20] and [21] were deemed negligible and so the values provided by all three were utilised. These are shown in Fig. 3, which clearly demonstrates the scarcity of experimental data, in particular for higher levels of hydrogen enrichment.

Chemical models provide more versatility compared to the experimental values, as s_{L0} can be calculated for any hydrogen enrichment value and any equivalence ratio. Two mechanisms were considered: the GRI-Mech3.0 [22] and the CRECK-NH3 [23]. The former is mostly used to model the combustion of hydrocarbon fuels (such as methane) and was used by [17] to calculate the unstretched laminar flame speed of methane-hydrogen flames. The latter is a detailed mechanism which focuses on the pyrolysis and oxidation of ammonia. No other mechanisms were used due to the constant advancement in the field of ammonia combustion simulation.

The two models were used together with the CANTERA [16] Python library to calculate s_{L0} at $\eta = \{0.333, 0.385, 0.455, 0.5, 0.545, 0.6\}$ and ϕ ranging from 0.6 to 1.375 at NTP conditions ($T_u = 293$ K and $P_u = 1$ atm). The calculation involved using a one-dimensional freely propagating premixed laminar flame model, provided by the CANTERA library, with the following grid refinement settings: ratio = 3, slope = 0.015 and curve = 0.03 (as used by [24]). These values were compared to those provided by [19] to confirm whether either model was suitable for ammonia-hydrogen flame speed calculations. For each value of η the overall percentage error was calculated using equation (10), where N is the number of ϕ at which s_{L0} was calculated for a specific η. The models were also used to calculate the s_{L0} necessary for the desired FTFs along with linearly interpolated values from the experimental data.

$$\%[Error] = 100 \times \frac{1}{N} \sum_{\phi} \frac{\left| s_{L0\ experimental} - s_{L0\ model} \right|}{s_{L0\ experimental}} \quad (10)$$

FTF calculation

The FTF gain was calculated by measuring the amplitude of the normalised heat release once it reached the limit cycle and dividing by the chosen constant normalised velocity perturbation

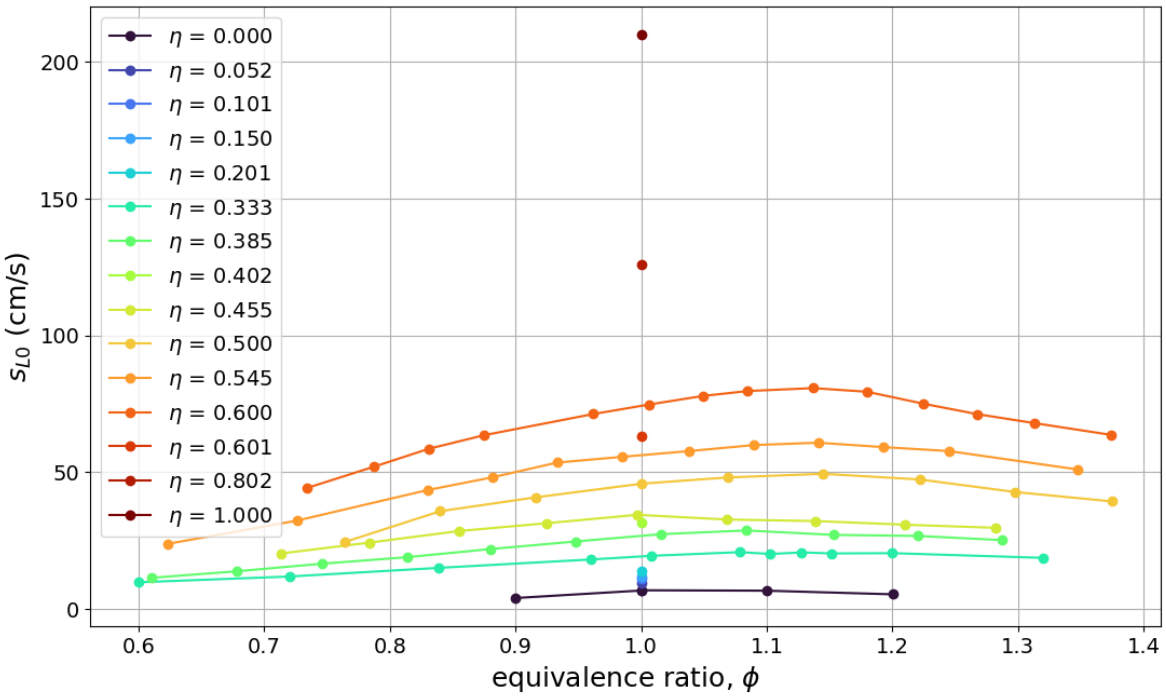

Fig. 3. All the experimental unstretched flame speeds obtained from [19-21] for different ϕ and η values.

amplitude, $\beta = 0.036$ (matching one used by [17] and [25]). The constant β implies the flame response was calculated independently from the forcing amplitude. The phase shift was calculated by cross-correlating the ratio of heat release function with the flow velocity perturbation function and then unwrapping the values obtained by either summing or subtracting 2π accordingly. To ensure smoother phase shift curves, 2π was then added again at a specific frequency if the difference between the phase shift at the specific frequency and the phase shift at the preceding frequency was higher than half of the difference between the adjusted phase shift (after 2π was added) and the preceding value.

The FTFs were calculated for $\eta = \{0.4, 0.6, 0.8\}$ and $\phi = 1.08$ fuel mixtures only. Due to time constraints, no lower values of η were used as ammonia's low flame speed led to much longer simulation times. No higher values of η were used due to hydrogen's high flame speed, as with $\bar{Q} = 2.69$ kW the flame would burn backwards (flashback occurs) rendering the simulation unsolvable. An equivalence ratio of 1.08 was chosen to match the value used by [17] and allow for comparison between the acoustic response of ammonia-hydrogen flames with the response of methane-hydrogen flames. Furthermore, NO_x emissions decrease as the equivalence ratio increases past stoichiometry for ammonia-hydrogen flames [19, 21, 26], which is of interest if using these fuel blends within gas turbines for more environmentally friendly energy production.

Five separate sets of simulations using the aforementioned values of η and ϕ were performed. The first three sets used interpolated experimental data, GRI-Mech3.0 and CRECK-NH3 to calculate s_{L0} respectively, each using a dummy value of $\mathcal{L} = 1$ mm for the Markstein length. The last two sets used $\mathcal{M} = 1$ and $\mathcal{M} = 2$ respectively, while s_{L0} and δ_f were calculated using the CRECK-NH3 model. The latter was calculated using the maximum temperature gradient across the reaction zone of the flame, $|dT/dz|_{max}$, as shown by equation (11), where T_u represents the unburned gas temperature, T_b the burned gas temperature, and z is the direction normal to the one-dimensional freely propagating premixed laminar flame [27].

$$\delta_f = \frac{T_b - T_u}{\left|\frac{dT}{dz}\right|_{max}} \tag{11}$$

The dummy values of $\mathcal{M}$ were chosen according to the experimental data from [19]. The data shows $\mathcal{M}$ varies between approximately -2 and 2 for flames with $\eta = \{0.5, 0.547, 0.584\}$ and $\phi = [0.6, 1.8]$. For rich fuel mixtures, however, $\mathcal{M}$ lies approximately between 0 and 2. Lee et al. [21], computed $\mathcal{M}$ for ammonia-hydrogen blends with $\eta = \{0.1, 0.3, 0.5\}$ and $\phi = [0.6, 1.6]$ but these values did not match those obtained from experimental work. As no accurate $\mathcal{M}$ could be found for all ammonia-hydrogen mixtures used in this work, the decision was made to utilise dummy values instead. As all simulations in this work use $\phi = 1.08$, $\mathcal{M} = 1$ and $\mathcal{M} = 2$ were deemed appropriate dummy values to ascertain the flame response sensitivity to $\mathcal{M}$, and therefore to $\mathcal{L}$.

The first three sets were compared between each other to ascertain the importance of an accurate s_{L0} when calculating the FTFs. The third set was then used to understand the effect of hydrogen enrichment on the flame response of ammonia hydrogen flames specifically. The last two sets were used to ascertain the importance of an accurate $\mathcal{M}$ when calculating the FTFs. The third set was also used to compare the flame response of the ammonia hydrogen flames to that of methane hydrogen flames [17].

FDF calculation

The non-linear flame transfer function, also called the flame describing function (FDF), is dependent on both the perturbation frequency, ω, and the normalised perturbation amplitude, β. A sixth set of

Table 1. Summary of the parameters changed throughout the simulations, all simulations use $\phi = 1.08$, $T_u = 293$ K and $P_u = 1$ atm

Set	s_{L0}	η	$\mathcal{L}$ (mm)	$\mathcal{M}$	β
1	Experimental	0.4, 0.6	1	-	0.036
2	GRI-Mech3.0	0.4, 0.6	1	-	0.036
3	CRECK-NH3	0.4, 0.6, 0.8	1	-	0.036
4	CRECK-NH3	0.4, 0.6	-	1	0.036
5	CRECK-NH3	0.4, 0.6	-	2	0.036
6	CRECK-NH3	0.6	1	-	0.036, 0.071, 0.0143, 0.214

simulations was conducted using $\beta = \{0.036, 0.071, 0.143, 0.214\}$, while $\eta = 0.6$ and $\phi = 1.08$, to analyse non-linear effects on the flame response. Matching values of β were also used by [17] for methane-hydrogen flames (numerical simulations) and by [25] for methane only flames (experimentally).

The FDF can be regarded as a set of FTFs for different β, as for small enough perturbations the flame response can be considered linear [18].

A summary of the parameters used in all six simulation sets is shown in table 1.

Results and Discussion

Experimental and modelled flame speed

Figure 3 compares the s_{L0} obtained from the experimental data [19-21] to those obtained through the chemical models. It shows s_{L0} increases as η increases, as hydrogen has a higher flame speed than ammonia. Furthermore, s_{L0} reaches a maximum at slightly rich conditions, when $\phi = 1.1$ approximately, for all values of η.

All graphs within Fig. 4 clearly show the inadequacy of the GRI-Mech3.0 model for ammonia-hydrogen flame simulations. The model always underpredicts s_{L0} with a percentage error exceeding 35%. This model focuses on hydrocarbon combustion and evidently lacks the necessary reactions to accurately model ammonia combustion. On the other hand, the CRECK-NH3 model always matched the experimental values to within 12% and was always more accurate than the GRI-Mech3.0 model. It is noted that CRECK-NH3 was specifically developed for ammonia pyrolysis and oxidation modelling.

Although the CRECK-NH3 model was shown to be significantly more accurate than the GRI-Mech3.0 model, the latter was still used to obtain the FTFs to ascertain the sensitivity of the FTF to flame speed. The GRI-Mech3.0 s_{L0} values acted as dummy values to better understand and highlight the sensitivity of the acoustic response to flame speed.

While it presented some degree of error, the CRECK-NH3 model was used in the calculation of the FTFs utilised to assess the acoustic response of ammonia and hydrogen flames as it provided more versatility than the experimental values.

Table 2. All the unstretched laminar flame speed values in m/s used in the calculation of the FTFs when $\phi = 1.08$

η	Experimental	CRECK-NH3	GRI-Mech3.0
0.4	0.2928	0.3122	0.1814
0.6	0.7931	0.7111	0.4890
0.8	-	1.3920	1.2750

Sensitivity of predicted flame acoustic response to flame speed

Table 2 contains the s_{L0} values obtained from either linear interpolation of experimental values [19-21] or from the chemical kinetic models when $\phi = 1.08$. The effect of the different s_{L0} values on the mean flame front is illustrated in Fig. 5. A higher s_{L0} leads to a shorter flame. This occurs for example when $\eta = 0.4$ and the CRECK-NH3 underpredicts s_{L0} compared to the experimental value. The same is verified when η increases, as a higher hydrogen content leads to a higher flame speed.

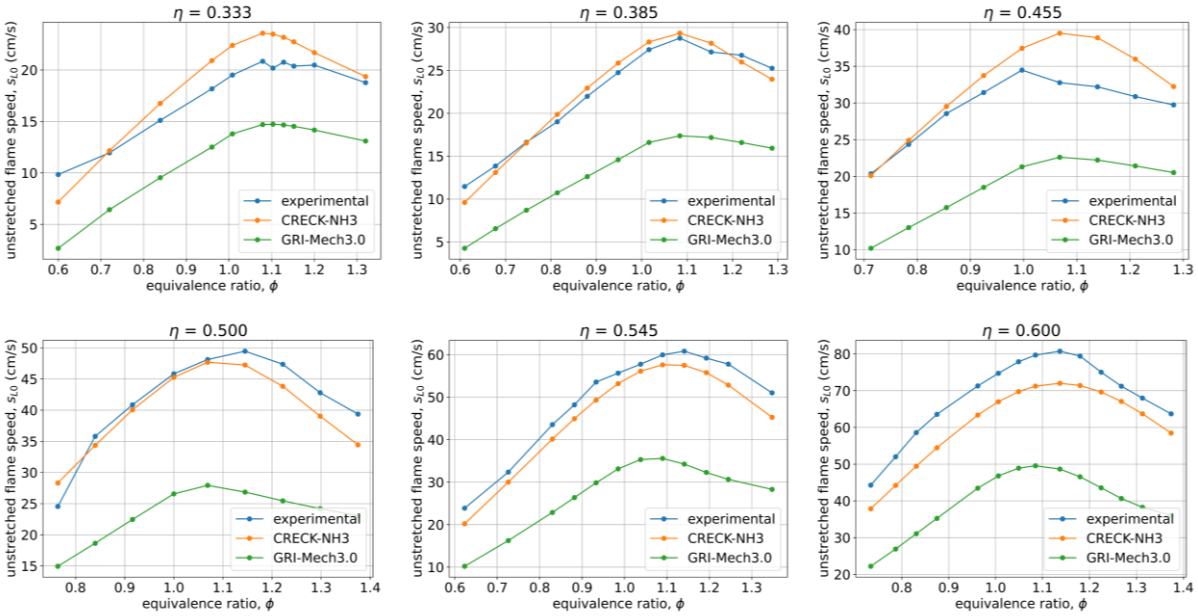

Fig. 4. Comparison between the unstretched laminar flame speed values obtained from the experimental data and from the CRECK-NH3 and the GRI-Mech3.0 chemical models.

To ascertain the effect of s_{L0} accuracy on the FTF, the values for $\eta = \{0.4, 0.6\}$ were used to calculate three sets of FTFs (using a dummy Markstein length of $\mathcal{L} = 1$ mm). These sets are shown in Figs. 6 and 7.

The FTF gain curves calculated using the CRECK-NH3 s_{L0} are far more similar to those using the experimental s_{L0} compared to the ones using the GRI-Mech-3.0 s_{L0}, with the errors being more accentuated for lower η. The same is seen for the phase shift graphs. Some minor differences in phase shift could also be attributed to the phase unwrapping method used. Overall, these figures highlight the importance of an accurate s_{L0} when calculating the FTFs.

The gain drop-off at lower frequencies for the GRI-Mech3.0 graphs was due to the lower value of s_{L0} (see table 2).

Lim, Li and Morgans [17] observed the frequency of the gain drop-off being pushed to higher frequencies as the hydrogen content increased. As hydrogen addition leads to an increase in s_{L0}, it is then possible to conclude a lower s_{L0} leads to an earlier gain drop-off, as shown by the GRI-Mech3.0 curves.

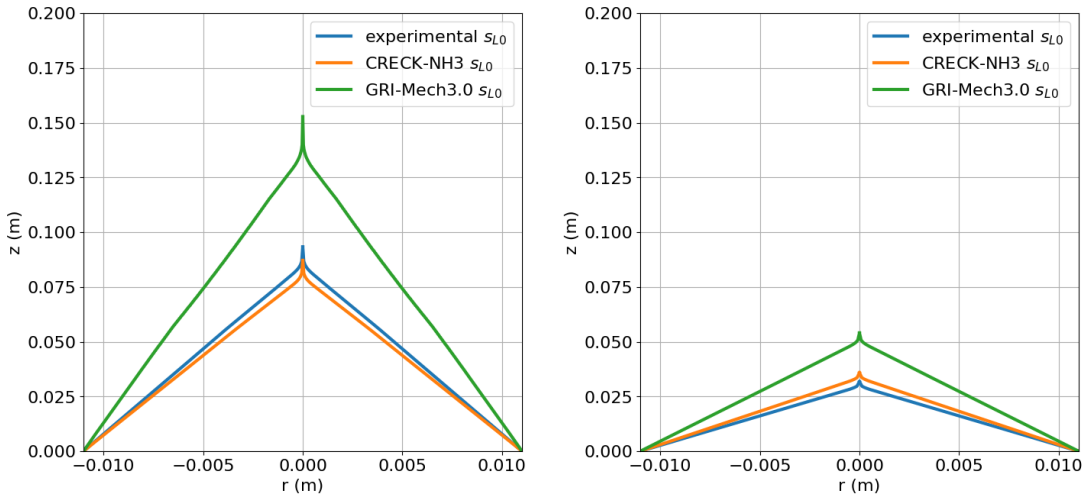

Fig. 5. Average flame front shape for $\eta = 0.4$ (left) and $\eta = 0.6$ (right) using experimental s_{L0} (blue), CRECK-NH3 s_{L0} (orange) and GRI-Mech3.0 s_{L0} (green) when $\phi = 1.08$, $\beta = 0.036$ and $f = 40\ Hz$

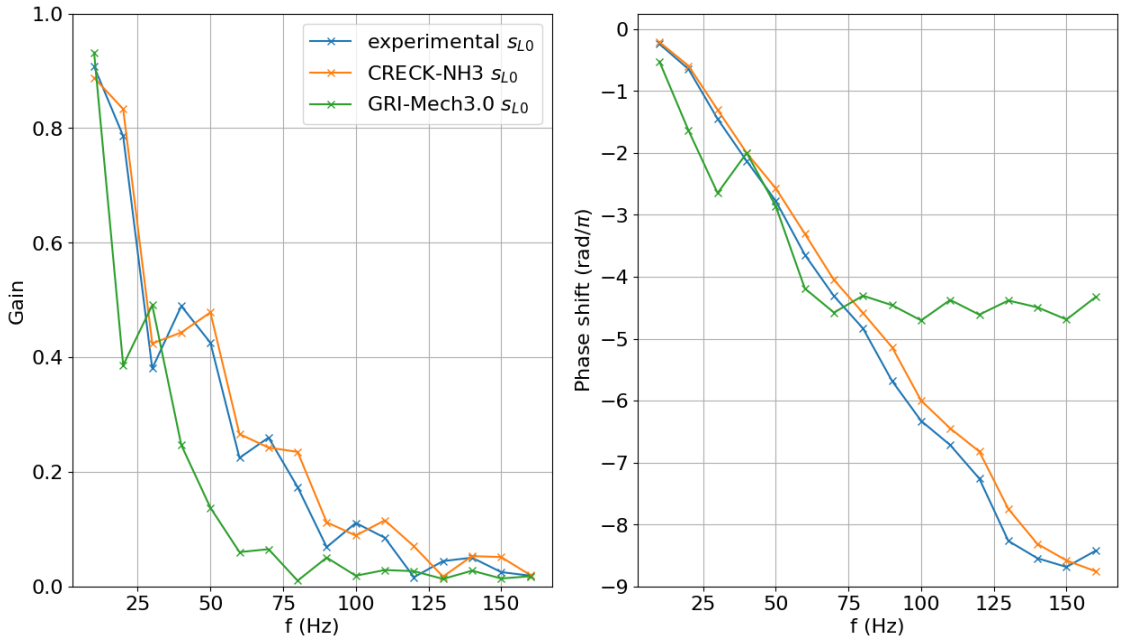

Fig. 6. FTF gain (left) and phase shift (right) for $\eta = 0.4$ using either the experimental s_{L0} (blue), the CRECK-NH3 s_{L0} (orange) or the GRI-Mech3.0 s_{L0} (green)

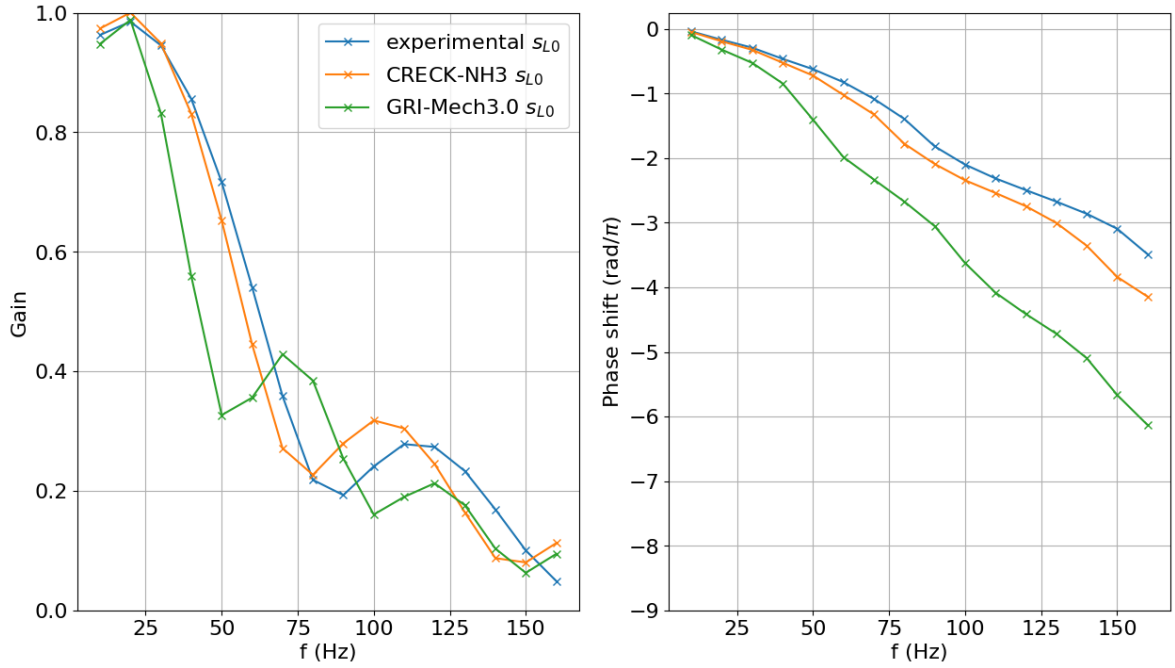

Fig. 7. FTF gain (left) and phase shift (right) for $\eta = 0.6$ using either the experimental s_{L0} (blue), the CRECK-NH3 s_{L0} (orange) or the GRI-Mech3.0 s_{L0} (green)

In both figures, the phase shift curves follow mostly the same trend, the phase lag increases as the forcing frequency increases, except for the curve corresponding to the GRI-Mech3.0 s_{L0} in Fig. 6. Instead, the phase shift remains somewhat constant once f > 75 Hz. The phase shift levels off once the gain reaches a low enough value (close to 0), which was also confirmed by [25] for pure methane flames at higher perturbation amplitudes. The slight increase in phase shift between f =30 Hz and f =40 Hz is due to the phase unwrapping method used.

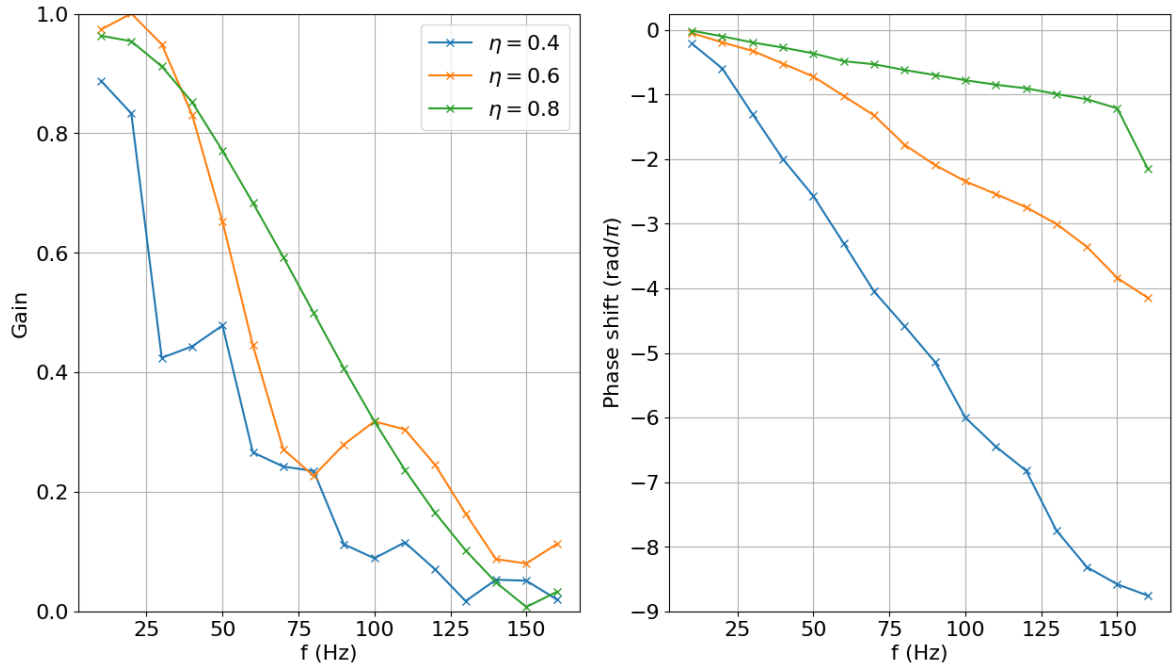

Fig. 8. FTF gain (left) and phase shift (right) calculated using CRECK-NH3 s_{L0} for $\eta = 0.4$ (blue), $\eta = 0.6$ (orange) and $\eta = 0.8$ (green)

Effect of hydrogen enrichment on FTF

The FTF set using the CRECK-NH3 s_{L0} was used to determine the effects of hydrogen enrichment on the acoustic response of ammonia flames. Figure 8 shows the FTF gain and phase shift corresponding to $\eta = \{0.4, 0.6, 0.8\}$. As the hydrogen content increases, and therefore so does s_{L0}, the gain drop-off occurs at higher frequencies, implying a higher propensity to thermoacoustic instabilities.

As η increases, the phase lag decreases and the relation between phase shift and forcing frequency becomes more linear, as shown in Fig. 8. The influence of phase shift on thermoacoustic instability is not as straightforward as that of gain, as the phase shift also interacts with the combustor geometry and its effects on the flame response will therefore depend on the specific combustor.

These same phenomena were also verified by [17] for methane-hydrogen flames.

Effect of Markstein length on FTF

Two more sets of FTFs were calculated using the CRECK-NH3 s_{L0}: one with $\mathcal{M} = 1$ and the other with $\mathcal{M} = 2$. Figure 9 shows the FTFs of this set when $\eta = \{0.4, 0.6\}$. Both the gain and phase shift curves are almost indistinguishable from each other at the same value of η. The minor differences in phase shift could also be attributed to the phase unwrapping method used. The FTFs therefore do not show great sensitivity to $\mathcal{M}$, and an approximation of $\mathcal{L}$ can be used in the case of laminar flames for solving the G-equation. A suggestion for this approximation would be the flame thickness, as $\mathcal{L}$ is of the same order as the flame thickness [15] and the latter can be easily calculated using chemical kinetic models. The same was verified by [17] for methane-hydrogen flames.

Ammonia hydrogen flames vs. methane hydrogen flames

The FTFs calculated using the CRECK-NH3 s_{L0} for $\eta = \{0.4, 0.6, 0.8\}$ were compared to the FTFs obtained by [17] for methane-hydrogen flames with the same hydrogen enrichment level. The s_{L0} of the ammonia and methane flames are shown in table 3 (the methane s_{L0} was calculated using the GRI-Mech3.0, as done by [17]).

The ammonia flame is slower than the methane flame for all values of η, except for $\eta = 0.8$. The reason for this is unknown, as one would expect the ammonia flame to always be slower than the methane flame for the same level of hydrogen enrichment, as a pure ammonia flame is significantly slower than a pure methane flame. This phenomenon has also been shown through experimental data. Under stoichiometric conditions, $P_u = 1$ bar and $T_u = 298$ K and with $\eta = 0.8$, [20] found $s_{L0} = 1.24$ m/s for ammonia-hydrogen flames. Under the same conditions, except at slightly higher temperature ($T_u = 303$ K), [28] found $s_{L0} = 1.17$ m/s for methane-hydrogen flames (with the same level of hydrogen enrichment). Although the difference between the experimental s_{L0} is not as significant as the difference between the calculated

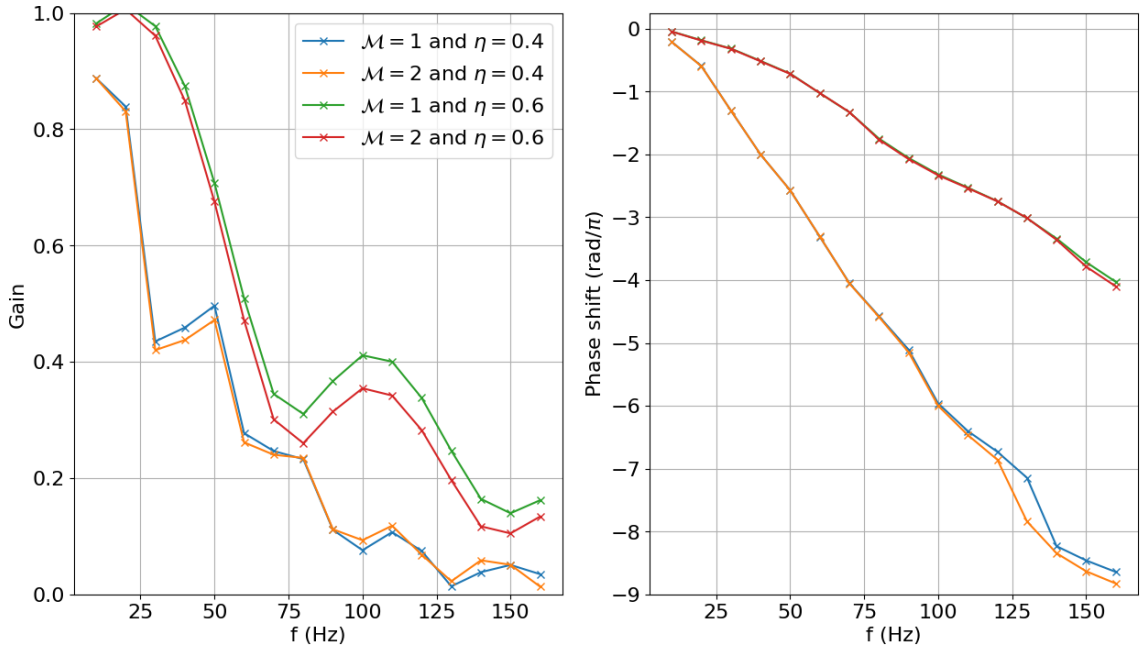

Fig. 9. FTF gain (left) and phase shift (right) calculated using CRECK-NH3 s_{L0} for $\mathcal{M} = 1$ and $\eta = 0.4$ (blue), $\mathcal{M} = 2$ and $\eta = 0.4$ (orange), $\mathcal{M} = 1$ and $\eta = 0.6$ (green) and $\mathcal{M} = 2$ and $\eta = 0.6$ (red)

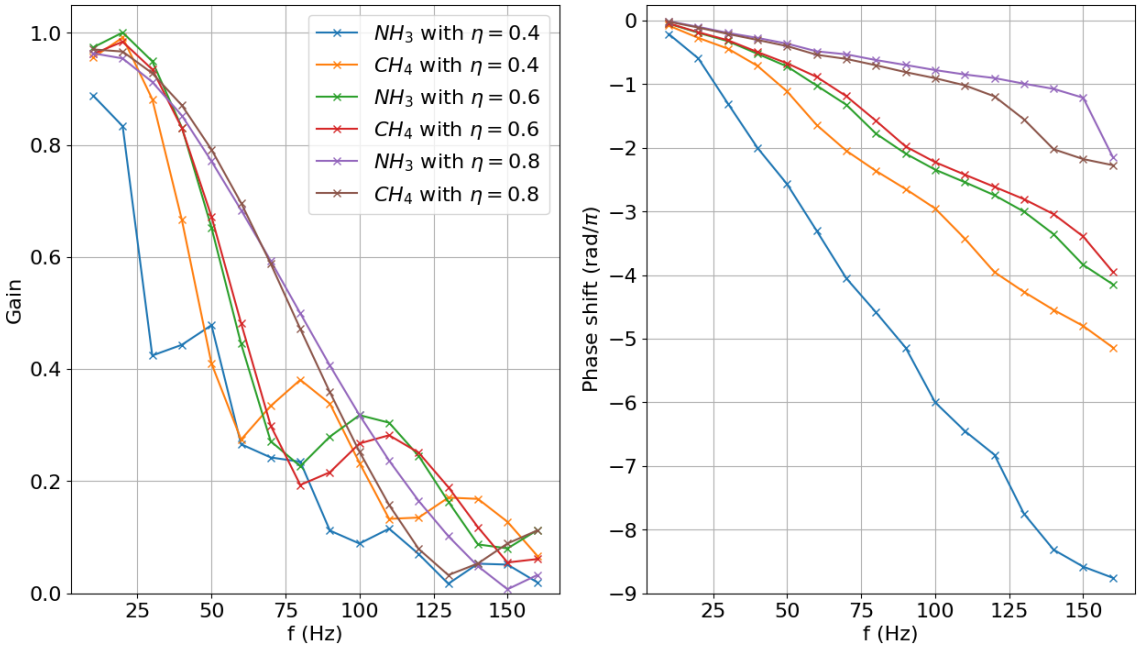

Fig. 10. FTF gain (left) and phase shift (right) calculated using CRECK-NH3 s_{L0} (ammonia) or GRI-Mech3.0 (methane) for ammonia flame with $\eta = 0.4$ (blue), methane flame with $\eta = 0.4$ (orange), ammonia flame with $\eta = 0.6$ (green), methane flame with $\eta = 0.6$ (red), ammonia flame with $\eta = 0.8$ (purple) and methane flame with $\eta = 0.8$ (brown)

s_{L0}, it still confirms the possibility of ammonia-hydrogen flames being faster than methane-hydrogen flames for the same level of hydrogen enrichment. A thorough investigation into this phenomenon was outside the scope of this research.

Table 3. Unstretched laminar flame speed in m/s of ammonia hydrogen and methane hydrogen flames with several levels of hydrogen enrichment when $\phi = 1.08$

η	**NH_3**	**CH_4**
0	0.0823	0.3859
0.4	0.3122	0.5538
0.6	0.7111	0.7523
0.8	1.3920	1.2175

For both the ammonia and methane mixtures, as η increases the gain drop-off occurs at higher frequencies, as shown in Fig. 10. The flame thus responds to acoustic waves of higher frequencies, likely to increase the propensity to combustor thermoacoustic instability. For the same level of hydrogen enrichment, the ammonia flame shows a weaker response to acoustic excitation compared to the methane flame, except for $\eta = 0.8$, once the ammonia flame speed is higher than the methane flame speed. The gain drop-off of the ammonia flame occurs at a higher frequency once $\eta = 0.8$ compared to the methane flame. This implies s_{L0} is the variable which most influences the flame response to acoustic perturbations.

The phase shift graphs for ammonia and methane flames, shown in Fig. 10, all show the same trend: as the hydrogen content increases, the phase lag decreases, and the response becomes more linear. The less difference there is between the s_{L0} value of the ammonia flame and the methane flame, the more similar the response to the acoustic perturbations of each flame is. The responses are most similar when $\eta = 0.6$ while they are most different when $\eta = 0.4$. This once again highlights the sensitivity of the flame response to s_{L0}.

Effect of velocity forcing nonlinearity

A brief analysis on non-linear effects on the flame response was also performed by calculating the flame describing function (FDF) when $\eta = 0.6$ and $\phi = 1.08$. This FDF is shown in figure 11.

The FDF is the non-linear version of the FTF and depends not only on the forcing frequency but also on the forcing amplitude (equation (12)). In these simulations, the forcing amplitude was varied between $\beta = \{0.036, 0.071, 0.143, 0.214\}$ to match the values used by both [17] and [25].

$$\mathcal{F}(\omega, \beta) = \frac{\frac{\dot{Q}'}{\bar{\dot{Q}}}}{\beta} \qquad (12)$$

Within Fig. 11, the gain curves at frequencies below 70 Hz are almost indistinguishable from each other,

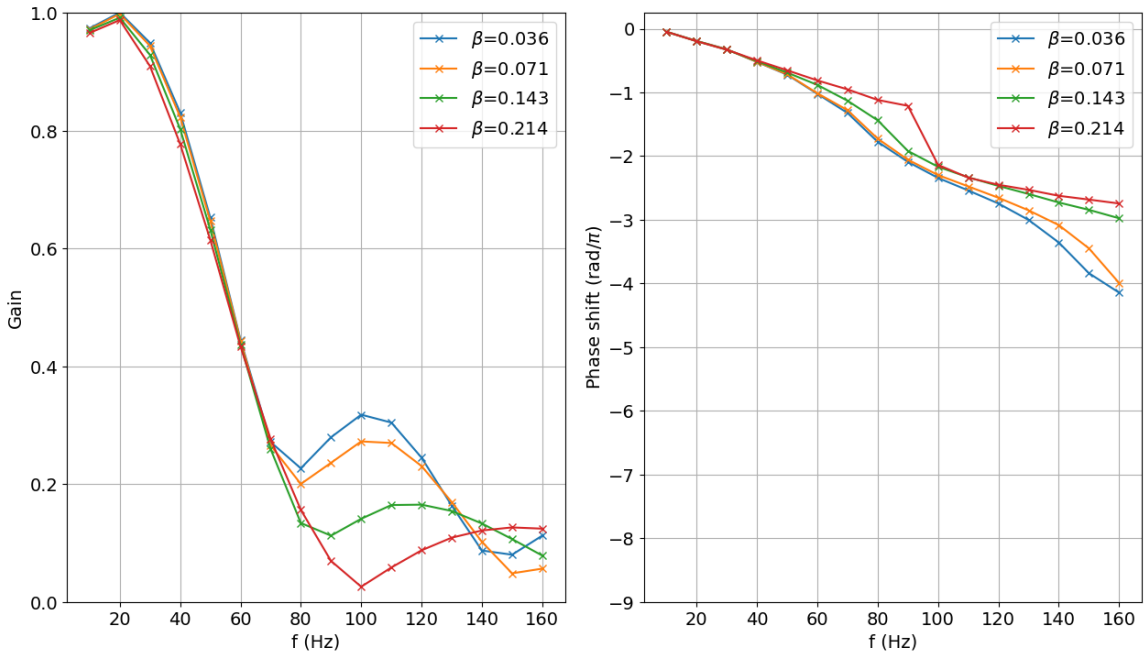

Fig. 11. FDF gain (left), and phase shift (right) calculated using CRECK-NH3 s_{L0} for ammonia hydrogen flames when $\eta = 0.6$ and $\phi = 1.08$ for different flow velocity perturbation amplitudes, $\beta = \{0.036, 0.071, 0.143, 0.214\}$

showing the flame response is independent of the forcing amplitude at lower frequencies, at this level of hydrogen enrichment. At low frequencies, the acoustic response is linear. Similarly to gain, phase shift is also independent on β at low frequencies, but also does not show great dependence at higher frequencies. Furthermore, the phase shift curves also show an increase in forcing amplitude leads to a decrease in phase lag. The same phenomena were found by [17] for hydrogen-methane flames and by [4] and [25] for pure methane flames.

Lim et al. [17] found an increase in the laminar flame speed led to a loss in the dependence of the acoustic response on the normalised velocity forcing amplitude at low frequencies for hydrogen-methane flames. The same should be true for hydrogen-ammonia flames, as many of the conclusions drawn by [17] for hydrogen-methane flames have also been confirmed for hydrogen-ammonia flames in this work, but further research is needed to confirm this.

Conclusion

Ammonia is a potential carbon-free fuel for energy production using gas turbines. The acoustic response of rich, $\phi = 1.08$, ammonia-hydrogen flames was assessed through the flame transfer function, calculated numerically by solving the G-equation.

Solving the G-equation requires knowing the flame speed value, s_L, which in turn requires the unstretched laminar flame speed, s_{L0}, and the Markstein length, $\mathcal{L}$, (flame strain effects were disregarded in this case). A dummy value of $\mathcal{L} = 1$ mm was used for most simulations, while s_{L0} was calculated from either experimental values available in literature or from either of two chemical kinetic models: the CRECK-NH3 and the GRI-Mech3.0. When comparing the modelled values to the experimental ones for the same ϕ and η, the CRECK-NH3 model was the more accurate model as it always presented an overall percentage error below 12% for all η values over a range of ϕ. Comparatively, the GRI-Mech3.0 mechanism consistently presented an error above 35%. This was expected, as the GRI-Mech3.0 focuses on hydrocarbon combustion while the CRECK-NH3 was developed for ammonia pyrolysis and oxidation simulation.

Several sets of FTFs were calculated using experimental or modelled s_{L0} and different dummy $\mathcal{M}$ values. The FTFs calculated using the CRECK-NH3 s_{L0} were more similar to those using the experimental s_{L0} compared to the ones using the GRI-Mech3.0 s_{L0}. The FTFs using different $\mathcal{M}$ were almost indistinguishable. These showed s_{L0} is the variable to which the FTF is most sensitive while $\mathcal{M}$ barely seems to affect the flame response.

The FTFs also showed flames with a high ammonia percentage and a low hydrogen enrichment level responded less strongly to acoustic excitation due to ammonia's lower flame speed. Consequently, as the hydrogen enrichment level was increased, and the flame speed also increased, the flames respond more strongly to acoustic excitation, as shown by the gain drop-off of the FTF which occurred at higher

frequencies. Furthermore, when compared to methane-hydrogen flames with the same level of hydrogen enrichment, the ammonia flames responded more weakly to acoustic excitation as long as s_{L0} was lower than the methane-hydrogen flames. These results imply the need for extra care when designing ammonia-hydrogen fuelled gas turbines, as an increase in hydrogen could lead to adverse effects due to propensity to thermoacoustic instabilities.

Conflicts of Interest

The authors declare no conflict of interest.

References

1. Zhang J, Ratner A. Experimental study of the effects of hydrogen addition on the thermoacoustic instability in a variable-length combustor. *Int J Hydrogen Energy.* 2021;46(29):16086-100. https://doi.org/10.1016/j.ijhydene.2021.02.063.

2. Candel S. Combustion dynamics and control: progress and challenges. *Proc combust inst*. 2002;29(1):1-28. https://doi.org/10.1016/S1540-7489(02)80007-4.

3. Noiray N, Durox D, Schuller T, Candel S. A unified framework for nonlinear combustion instability analysis based on the flame describing function. *J Fluid Mech.* 2008;615:139-67. https://doi.org/10.1017/S0022112008003613.

4. Kashinath K, Hemchandra S, Juniper MP. Nonlinear Phenomena in Thermoacoustic Systems With Premixed Flames. *J Eng Gas Turbines Power*. 2013 05;135(6). 061502. https://doi.org/10.1115/1.4023305.

5. Jones R, Goldmeer J, Monetti B. Addressing gas turbine fuel flexibility. GE Energy. 2011;4601:1-20.

6. Valera-Medina A, Xiao H, Owen-Jones M, David WIF, Bowen PJ. Ammonia for power. *Prog Energy Combust Sci.* 2018;69:63-102. https://doi.org/10.1016/j.pecs.2018.07.001.

7. Katoch A, Guiberti TF, de Campos DV, Lacoste DA. Dual-fuel, dual-swirl burner for the mitigation of thermoacoustic instabilities in turbulent ammonia-hydrogen flames. *Combust Flame*. 2022;12;246:112392. https://doi.org/10.1016/j.combustflame.2022.112392.

8. Peng D, Merriman B, Osher S, Zhao H, Kang M. A PDE-Based Fast Local Level Set Method. *J Comp Phys.*1999;155(2):410-38. https://doi.org/10.1006/jcph.1999.6345.

9. Peters N. Premixed turbulent combustion. In: Turbulent combustion. Cambridge Monographs on Mechanics, Eds.; Cambridge University Press; United Kingdom, 2000. pp. 91–98. https://doi.org/10.1017/CBO9780511612701.003.

10. Fleifil M, Annaswamy AM, Ghoneim Z, Ghoniem AF. Response of a laminar premixed flame to flow oscillations: A kinematic model and thermoacoustic instability results. *Combust Flame.* 1996;106(4):487-510. https://doi.org/10.1016/0010-2180(96)00049-1.

11. Luzzato CM, Assier R, Morgans A, Wu X. Modelling thermo-acoustic instabilities of an anchored laminar flame in a simple lean premixed combustor: including hydrodynamic effects. In: 19th AIAA/CEAS Aeroacoustics Conference; 2013. p. 2003. https://doi.org/10.2514/6.2013-2003.

12. Dowling AP. Nonlinear self-excited oscillations of a ducted flame. *J Fluid Mech.* 1997;346:271–290. https://doi.org/10.1017/S0022112097006484.

13. Dowling AP. A kinematic model of a ducted flame. *J Fluid Mech*. 1999;394:51–72. https://doi.org/10.1017/S0022112099005686.

14. Li J, Morgans AS. Feedback control of combustion instabilities from within limit cycle oscillations using H loop-shaping and the ν-gap metric. *Proc Royal Society A: Math Phys Eng Sci*. 2016;472(2191):20150821. https://doi.org/10.1098/rspa.2015.0821.

15. Markstein GH. Chapter B - Theory of Flame Propagation. In: Nonsteady Flame Propagation, Markstein GH, Eds.; Elsevier; 1964; Volume 75, pp. 5-14. https://doi.org/10.1016/B978-1-4831-9659-6.50005-6.

16. Goodwin DG, Moffat HK, Speth RL. Cantera: An Object-oriented Software Toolkit for Chemical Kinetics, Thermodynamics, and Transport Processes. Version 2.3.0. Zenodo; 2017.

17. Lim Z, Li J, Morgans AS. The effect of hydrogen enrichment on the forced response of CH4/H2/Air laminar flames. *Int J Hydrogen Energy*. 2021;46(46):23943-53. https://doi.org/10.1016/j.ijhydene.2021.04.171.

18. Schuller T, Ducruix S, Durox D, Candel S. Modeling tools for the prediction of premixed flame transfer functions. *Proc Combust Inst.* 2002;29(1):107-13. https://doi.org/10.1016/S1540-7489(02)80018-9.

19. Li J, Huang H, Kobayashi N, He Z, Nagai Y. Study on using hydrogen and ammonia as fuels: Combustion characteristics and NOx formation. *Int J Energy Res.* 2014 7;38:1214-23. https://doi.org/10.1002/er.3141.

20. Ichikawa A, Hayakawa A, Kitagawa Y, Somarathne KDKA, Kudo T, Kobayashi H. Laminar burning velocity and Markstein length of ammonia/hydrogen/air premixed flames at elevated pressures. *Int J Hydrogen Energy*. 2015 8;40: 9570-8. https://doi.org/10.1016/j.ijhydene.2015.04.024.

21. Lee JH, Kim JH, Park JH, Kwon OC. Studies on properties of laminar premixed hydrogen-added ammonia/air flames for hydrogen production. *Int J Hydrogen Energy*. 20102;35:1054-64. https://doi.org/10.1016/j.ijhydene.2009.11.071.

22. Smith GP, Golden DM, Frenklach M, Moriarty NW, Eiteneer B, Goldenberg M, et al.. GRI-Mech 3.0; 1999. Available from: http://www.me.berkley.edu/gri_mech/
23. Stagni A, Cavallotti C, Arunthanayothin S, Song Y, Herbinet O, Battin-Leclerc F, et al.. NH3 mechanism;. Available from: http://creckmodeling.chem.polimi.it/menu-kinetics/menu-kinetics-special-mechanisms/menu-kinetics-nh3-mechanism.
24. Goldmann A, Dinkelacker F. Approximation of laminar flame characteristics on premixed ammonia/hydrogen/nitrogen/air mixtures at elevated temperatures and pressures. *Fuel*. 2018;224:366-78. https://doi.org/10.1016/j.fuel.2018.03.030.
25. Durox D, Schuller T, Noiray N, Candel S. Experimental analysis of nonlinear flame transfer functions for different flame geometries. *Proc Combust Inst.* 2009;32(1):1391-8. https://doi.org/10.1016/j.proci.2008.06.204.
26. Effects of ammonia substitution on combustion stability limits and NOx emissions of premixed hydrogen–air flames. *Int J Hydrogen Energy*. 2012;37(8):6933-41. https://doi.org/10.1016/j.ijhydene.2012.01.059.
27. Poinsot T, Veynante D. In: Theoretical and numerical combustion. RT Edwards, Inc.; 2005. p. 56-58; doi: https://doi.org/10.1002/0470091355.ecm067
28. Hu E, Huang Z, He J, Jin C, Zheng J. Experimental and numerical study on laminar burning characteristics of premixed methane–hydrogen–air flames. *Int J Hydrogen Energy*. 2009; 6;34:4876-88. https://doi.org/10.1016/j.ijhydene.2009.03.058.